

Cool white dwarf companions to four millisecond pulsars

C. G. Bassa^{1*}, J. Antoniadis², F. Camilo³, I. Cognard⁴, D. Koester⁵,
M. Kramer^{6,7}, S. R. Ransom⁸, B. W. Stappers⁷

¹*ASTRON, the Netherlands Institute for Radio Astronomy, Postbus 2, 7900 AA, Dwingeloo, the Netherlands*

²*Dunlap Institute for Astronomy and Astrophysics, University of Toronto, 50 St. George Street, Toronto, Ontario M5S 3H4, Canada*

³*Columbia Astrophysics Laboratory, Columbia University, New York, NY 10027, USA*

⁴*Station de Radioastronomie de Nançay, Observatoire de Paris, 18330 Nançay, France*

⁵*Institut für Theoretische Physik und Astrophysik, University of Kiel, D-24098 Kiel, Germany*

⁶*Max Planck Institut für Radioastronomie, Auf dem Hügel 69, 53121 Bonn, Germany*

⁷*Jodrell Bank Centre for Astrophysics, The University of Manchester, Manchester, M13 9PL, United Kingdom*

⁸*National Radio Astronomy Observatory, Charlottesville, VA 22903, USA*

Accepted 2015 November 2. Received 2015 October 9; in original form 2015 August 28

ABSTRACT

We report on photometric and spectroscopic observations of white dwarf companions to four binary radio millisecond pulsars, leading to the discovery of companions to PSRs J0614–3329, J1231–1411 and J2017+0603. We place limits on the brightness of the companion to PSR J0613–0200. Optical spectroscopy of the companion to PSR J0614–3329 identifies it as a DA type white dwarf with a temperature of $T_{\text{eff}} = 6460 \pm 80$ K, a surface gravity $\log g = 7.0 \pm 0.2$ cgs and a mass of $M_{\text{WD}} = 0.24 \pm 0.04 M_{\odot}$. We find that the distance to PSR J0614–3329 is smaller than previously estimated, removing the need for the pulsar to have an unrealistically high γ -ray efficiency. Comparing the photometry with predictions from white dwarf cooling models allows us to estimate temperatures and cooling ages of the companions to PSRs J0613–0200, J1231–1411 and J2017+0603. We find that the white dwarfs in these systems are cool $T_{\text{eff}} < 4000$ K and old $\gtrsim 5$ Gyr. Thin Hydrogen envelopes are required for these white dwarfs to cool to the observed temperatures, and we suggest that besides Hydrogen shell flashes, irradiation driven mass loss by the pulsar may have been important.

Key words: binaries: close – pulsars: general – white dwarfs – stars: individual: PSR J0613–0200, PSR J0614–3329, PSR J1231–1411, PSR J2017+0603

1 INTRODUCTION

Over the last few years the number of Galactic radio millisecond pulsars has increased dramatically (Ransom 2013). This increase is due to improved hardware used in all-sky pulsar searches at the Arecibo (Cordes et al. 2006), Green Bank (Hessels et al. 2008; Boyles et al. 2013), Parkes (Keith et al. 2010) and Effelsberg (Barr et al. 2013) telescopes, as well as targeted searches for pulsars associated with unidentified γ -ray sources recently discovered by the *Fermi* γ -ray space telescope (see Ray et al. 2012 for a summary and references).

Prior to these blind and targeted surveys the majority of millisecond pulsar binary companions located in the Galactic field (outside of globular clusters) were either low-mass ($0.1\text{--}0.4 M_{\odot}$) or intermediate mass ($0.4\text{--}1.1 M_{\odot}$) white

dwarfs, with the exception of two exotic ‘black widow’ pulsars with very low-mass (a few $0.01 M_{\odot}$) binary companions (van Kerkwijk et al. 2005). The new discoveries have shown us these exotic binary systems are in fact more common place, and even led to the addition of another class of binary companions, the ‘redback’ systems (Roberts 2013). The binary companions in the latter class have masses in a similar range as the low-mass white dwarfs ($0.1\text{--}0.4 M_{\odot}$), but are typically in compact orbits ($P_b < 1$ d). Both the black widow and redback systems are characterized by their compact orbits and eclipses of the radio signal due to material being ablated from the companion due to irradiation by the wind from the energetic pulsar. Furthermore, three of the redback systems have now been observed to transition back-and-forth between the rotation-powered pulsar state and an accretion-powered low-mass X-ray binary phase (Archibald et al. 2009; Papitto et al. 2013; Bassa et al. 2014), provid-

* bassa@astron.nl

Table 1. Properties of the pulsars under investigation. Distances d_{DM} are estimated from the observed dispersion measure (DM) and the Galactic extinction model of [Cordes & Lazio \(2002\)](#). Characteristic ages (τ_c) and spindown luminosities (L_{SD}) are estimated from the observed spin period P and the intrinsic spin period derivative \dot{P}_{int} , which is the observed spin period derivative corrected for the [Shklovskii \(1970\)](#) effect. Minimum and median companion masses are estimated assuming a $1.4 M_{\odot}$ pulsar and orbital inclinations of $i = 90^\circ$ for $m_{c,\text{min}}$ and $i = 60^\circ$ for $m_{c,\text{med}}$. The theoretical P_b - M_c relation by [Lin et al. \(2011\)](#) is used for the predicted companion mass $M_{c,\text{pred}}$. The P_b - M_c relation by [Tauris & Savonije \(1999\)](#) predicts companion masses that are $0.016 M_{\odot}$ heavier. The positional offsets $\Delta\alpha$ and $\Delta\delta$ denote the offset in position with respect to the pulsar.

Parameter	PSR J0613–0200	PSR J0614–3329	PSR J1231–1411	PSR J2017+0603
Spin period P (ms)	3.061844	3.148670	3.683879	2.896216
Period derivative \dot{P}_{int}	9.590×10^{-21}	1.74×10^{-20}	2.26×10^{-20}	8.0×10^{-21}
Dispersion measure DM (pc cm^{-3})	38.775	37.049	8.090	23.918
DM distance d_{DM} (kpc)	1.70	1.90	0.44	1.56
Spindown age τ_c (Gyr)	5.5	2.8	2.6	5.6
Spindown luminosity L_{SD} (erg s^{-1})	1.2×10^{34}	2.2×10^{34}	6.1×10^{33}	1.3×10^{34}
Orbital period P_b (d)	1.1985	53.585	1.8601	2.1985
Projected semi-major axis $a \sin i$ (s)	1.0914	27.639	2.0426	2.1929
Minimum companion mass $M_{c,\text{min}}$ (M_{\odot})	0.132	0.282	0.188	0.180
Median companion mass $M_{c,\text{med}}$ (M_{\odot})	0.153	0.332	0.220	0.211
Predicted companion mass $M_{c,\text{pred}}$ (M_{\odot})	0.188	0.299	0.198	0.201
References	1	2, 3, 4	2, 3	3, 4, 5
Derived parameters				
Companion right ascension α_{J2000}	...	06 ^h 14 ^m 10 ^s .348(8)	12 ^h 31 ^m 11 ^s .32(1)	20 ^h 17 ^m 22 ^s .706(8)
Companion declination δ_{J2000}	...	−33°29′53″.97(9)	−14°11′43″.43(16)	+06°03′05″.72(18)
Offset in right ascension ($\Delta\alpha$)	...	+0″.00(10)	+0″.21(18)	+0″.02(13)
Offset in declination ($\Delta\delta$)	...	+0″.15(9)	+0″.24(17)	+0″.15(18)
g' -band magnitude	> 24.7	22.11(1)	25.5(1)	25.30(9)
r' -band magnitude	> 23.8	21.77(1)	23.91(4)	24.0(2)
i' -band magnitude	> 23.7	21.69(1)	23.52(7)	24.24(7)
Effective temperature T_{eff} (K)	$\lesssim 4000$	6460 ± 80	~ 3000	$\lesssim 2500$
White dwarf cooling age τ_{WD} (Gyr)	$\gtrsim 5$	1–1.5	5–8	9–12
White dwarf distance d (kpc)	...	0.54–0.63	0.39–0.48	< 0.5

References: (1) [Desvignes et al. \(2015\)](#); (2) [Ransom et al. \(2011\)](#); (3) [Guillemot et al. \(2015\)](#); (4) [Arzoumanian et al. \(2015\)](#); (5) [Cognard et al. \(2011\)](#)

ing vital clues for the physics involved in the formation of millisecond pulsar binaries.

Optical observations of binary companions to millisecond pulsars allow independent measurements of millisecond pulsar and binary parameters. For the irradiated companions in black widow and redback systems, modelling of the orbitally modulated light curves constrains the companion temperatures, the orbital inclination and the irradiation efficiency of the companion by the pulsar wind (see [Breton et al. 2013](#) and references therein). For systems with white dwarf companions the companion temperature can be determined from photometry, allowing independent constraints on the white dwarf cooling age and the distance. The radial velocity curve and the atmospheric parameters of bright white dwarfs can be measured through optical spectroscopy, which determine the mass of the white dwarf and the pulsar (see [van Kerkwijk et al. 2005](#) for a review).

Here we report on optical observations of four energetic binary millisecond pulsars which are seen in γ -rays by *Fermi*. The parameters of these binary pulsars are listed in Table 1. Of the four, PSR J0613–0200 was already independently discovered by [Lorimer et al. \(1995\)](#), while PSRs J0614–3329, J1231–1411 and J2017+0603 were discovered in targeted searches of unassociated sources found by the *Fermi* LAT instrument ([Ransom et al. 2011](#); [Cognard et al. 2011](#)). The orbital parameters of the systems constrain the companion

masses to the range of 0.1 to $0.4 M_{\odot}$, and the absence of radio eclipses suggests that they are white dwarfs.

2 OBSERVATIONS AND DATA ANALYSIS

The fields of PSRs J0613–0200, J0614–3329, J1231–1411 and J2017+0603 were observed with the Gemini Multi-Object Spectrograph (GMOS) on the 8 m Gemini South telescope in Chile during the fall and winter of 2010/2011. The GMOS instrument uses three 2048×4608 pixel CCDs and with a pixel scale of $0''.073 \text{ pix}^{-1}$ they provide a vignetted field-of-view of $5'.5 \times 5'.5$. For these observations only data from the center CCD was used providing a field-of-view of $2'.5 \times 5'.5$. The CCD was read using 2×2 binning with a scale of $0''.146 \text{ pix}^{-1}$. Sets of dithered images were obtained in the Sloan g' , r' and i' filters ([Fukugita et al. 1996](#)) with 4 min exposures for PSRs J0614–3329, J1231–1411 and J2017+0603. Shorter exposures of 30 sec, 1 min and 2 min were obtained for PSR J0613–0200 to prevent a nearby star ([van Kerkwijk et al. 2005](#)) from saturating. For the astrometric and photometric calibration, short, 5 to 30 s exposures using all three filters were obtained for all three sources under photometric conditions. Flatfield frames were obtained during twilight through the standard Gemini calibration plan. The seeing during the observations varied between $0''.7$ to $1''.1$.

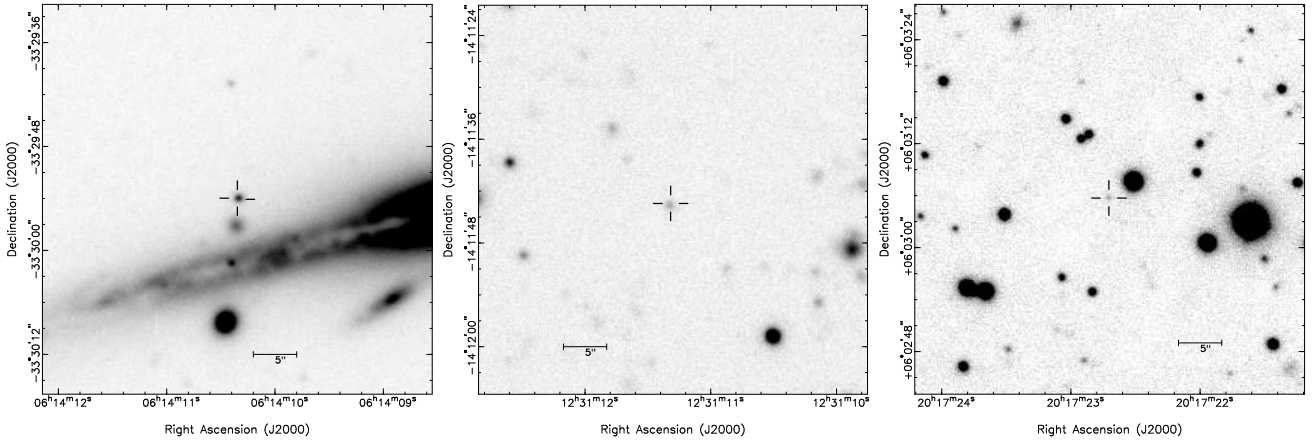


Figure 1. Images of the fields of PSRs J0614–3329 (left), J1231–1411 (middle) and J2017+0603 (right). Each image is $45'' \times 45''$ in size. The image of J2017+0603 is in i' , the others are in r' . The optical counterpart of each pulsar is indicated with $1''$ long tick marks.

Long-slit spectroscopy of the counterpart to PSR J0614–3329 was obtained with FORS2 at the ESO VLT. Two exposures with integration times of 3600 s and 3000 s were obtained on 2011 December 20 and 21 using the 1200B grism covering the wavelength range from 3730 to 5190 Å. A $1''$ slit was used with 2×2 binning, yielding a resolution of 2.8 Å , sampled at 0.71 Å pix^{-1} . The seeing during these observations varied between $0''.7$ and $1''.1$. In both observations the slit was placed such to include the three point-like sources South of the companion, as well as some of the emission from a background galaxy (see Fig. 1).

2.1 Astrometry

Stars on the short (5 to 30 s) r' images of each field were matched against stars in the 2MASS (Skrutskie et al. 2006; for PSRs J0613–0200, J0614–3329 and J2017+0603) or USNO-B1 (Monet et al. 2003; for PSR J1231–1411) catalogs for astrometric calibration. Fitting for a zero-point offset and a 4 parameter transfer matrix, an astrometric solution for each pulsar was determined having rms residuals ranging from $0''.1$ to $0''.2$ in each coordinate. For each pulsar the astrometric solution was transferred to the median combined images using a few dozen stars common to both images with considerably smaller rms residuals of $0''.02$ in both coordinates.

The calibrated images were searched for optical counterparts consistent with the pulsar timing positions. In the case of PSR J0613–0200 we use the timing position and proper motion of Desvignes et al. (2015), which yields $\alpha_{J2000} = 06^{\text{h}} 13^{\text{m}} 43^{\text{s}}.9760$ and $\delta_{J2000} = -02^{\circ} 00' 47''.241$ for the epoch of the GMOS observations. The uncertainty on the position is negligible. Ransom et al. (2011) provides timing positions for PSRs J0614–3329 and J1231–1411, of which the latter has a somewhat uncertain proper motion which places the pulsar at $\alpha_{J2000} = 12^{\text{h}} 31^{\text{m}} 11^{\text{s}}.305(2)$ and $\delta_{J2000} = -14^{\circ} 11' 43''.67(6)$ at the time of the optical observations. Using the more accurate proper motion by Guillemot et al. (2015) yields a consistent position. For PSR J2017+0603 we use the position from Cognard et al. (2011).

Optical counterparts are present in the 95% confidence error regions of the timing positions of J0614–3329,

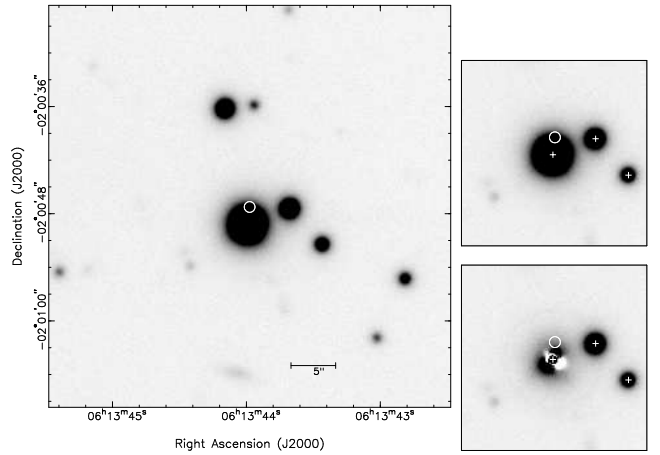


Figure 2. Images of the field containing PSR J0613–0200. The left-hand panel shows a $45'' \times 45''$ subsection of the averaged r' -band image. The radio timing position of PSR J0613–0200 is indicated with the $0''.6$ (99% confidence) error circle. The two right-hand panels show a $20'' \times 20''$ subsection of the same image, where in the bottom panel the stellar profile of the nearby star is removed. No counterpart is visible within the error circle.

J1231–1411 and J2017+0603 (see Fig. 1). The celestial position and observed $g'r'i'$ magnitudes of the counterparts are given in Table 1. In the case of PSR J0613–0200 the pulsar position is offset by $1''.9$ from a nearby unassociated star, having $r' = 15.6$. No counterpart is present in the $0''.60$ (99% confidence) error circle, see Fig. 2.

2.2 Photometry

The images were reduced using standard methods, where all images were corrected for bias from the overscan regions and flatfielded using the twilight flats. The images taken with the i' filter suffered from fringing. To correct for this, a fringe frame was created by median combining all 4 min i' images of PSR J2017+0603 and PSR J0614–3329 such that it contained only the contributions of the sky and the fringe variations. The level of the sky was estimated and subtracted,

and the remaining fringe variations were scaled and used to remove the fringes from the individual i' images. Finally, the dithered images in each filter were aligned using integer pixel offsets and median combined to increase the overall signal-to-noise.

The DAOPHOTII package (Stetson 1987) was used to determine instrumental magnitudes of stars on the images through point-spread-function (PSF) fitting. Aperture photometry of several bright stars was used to determine aperture corrections. For the photometric calibration we determined and compared instrumental magnitudes of stars in three standard fields (060000–300000, T Phe and PG 0942–029), observed in October and November 2010 as part of the standard GMOS calibration plan, against calibrated $g'r'i'$ magnitudes from the updated catalog¹ of Smith et al. (2002). Fitting for zero-point and color-coefficient, assuming standard GMOS extinction coefficients of 0.18, 0.10 and 0.08 mag per airmass for g' , r' and i' , respectively, we obtained rms residuals of 0.05 mag in g' , 0.02 mag in r' and 0.04 mag in i' .

Limits on the magnitude of a counterpart to PSR J0613–0200, located in the wings of the nearby star, were computed by performing photometry on copies of the original image with an artificial star inserted on the position of the pulsar. By varying the magnitude of the artificial star, 5σ detection limits were derived. These are listed in Table 1.

Finally, we checked for variability of the detected counterparts by comparing instrumental magnitudes obtained from the individual frames. For the counterpart to PSR J0614–3329 we do not find significant variability down to rms scatter of less than 0.05 mag in all three filters. This scatter is comparable to the scatter seen in stars of similar brightness. The counterparts to PSRs J1231–1411 and J2017+0603 are considerably fainter and not detected in each individual frame. As such, we set a conservative limit on the variability of the counterparts in these two systems at less than 0.3 mag in all three filters.

2.3 Spectroscopy

The spectra were corrected for bias by subtracting a master bias frame and flatfielded using lamp-flats. The spectrum of the companion was optimally extracted using a variation on the algorithms by Horne (1986) and Hynes (2002) to separate the flux from the companion from that of the nearby object by modelling their wavelength dependent spatial profiles. The wavelength scale was calibrated against arc lamp exposures taken during daytime. For the flux calibration we used an observation of the spectrophotometric standard GD 108 taken as part of the normal VLT calibration program. This calibration is approximate, as no correction for slit losses was applied. Based on the width of the slit and the seeing during the PSR J0614–3329 observations, at least 95% of the flux is accounted for.

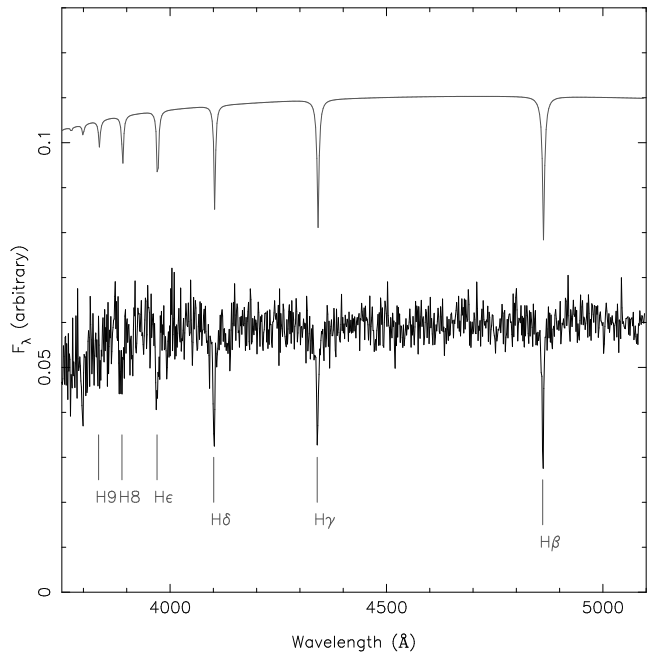


Figure 3. The spectrum of the counterpart to PSR J0614–3329. The lower curve shows the average of the two VLT spectra, shifted to zero velocity. Hydrogen lines in the Balmer series are seen from $H\beta$ upto $H9$, consistent with a DA type white dwarf. The top curve is a white dwarf atmosphere model with $T_{\text{eff}} = 6500$ K and $\log g = 7.0$ cgs, broadened by a truncated Gaussian representing the response of the slit and seeing and scaled to fit the observed spectrum. This model lies closest in the grid of atmosphere models used to the best fit values of $T_{\text{eff}} = 6460 \pm 80$ K and $\log g = 7.0 \pm 0.2$ cgs. Note that the model spectrum has been shifted upwards by 0.05 units.

3 RESULTS

We have found optical counterparts to PSR J0614–3329, PSR J1231–1411 and PSR J2017+0603. Given the density of stars in these fields, we estimate that the probability of finding a star in the error circle of these objects by chance is only a few percent. As such, we treat the optical counterparts to these millisecond pulsars as their binary companions in the remainder of the paper.

In the case of PSR J0614–3329, the optical spectrum of the counterpart (Fig. 3) shows the $H\beta$ to $H9$ hydrogen Balmer lines, classifying it as a DA type white dwarf, confirming it is the binary companion. The effective temperature and the surface gravity can be constrained by comparison of the observed spectrum with a grid of theoretical Hydrogen atmosphere models appropriate for DA type white dwarfs. This grid, an update of that presented in Koester (2010), spans temperatures of $T_{\text{eff}} = 6000$ to 7500 K and surface gravities of $\log g = 6.0$ to 8.5 cgs, with steps of 250 K and 0.25 dex. Using the fitting method described in Bassa et al. (2006b), the atmospheric parameters are constrained to $T_{\text{eff}} = 6460 \pm 80$ K and $\log g = 7.0 \pm 0.2$ cgs.

Interpolating between the discrete mass models by Panei et al. (2007), these atmospheric parameters correspond to a white dwarf mass of $M_{\text{WD}} = 0.24 \pm 0.04 M_{\odot}$. The minimum companion mass for an edge on orbit and a $1.4 M_{\odot}$ pulsar is $0.282 M_{\odot}$ ($M_{\text{c,min}}$ in Table 1), while the P_b -

¹ http://www-star.fnal.gov/Southern_ugriz/www/Fieldindex.html

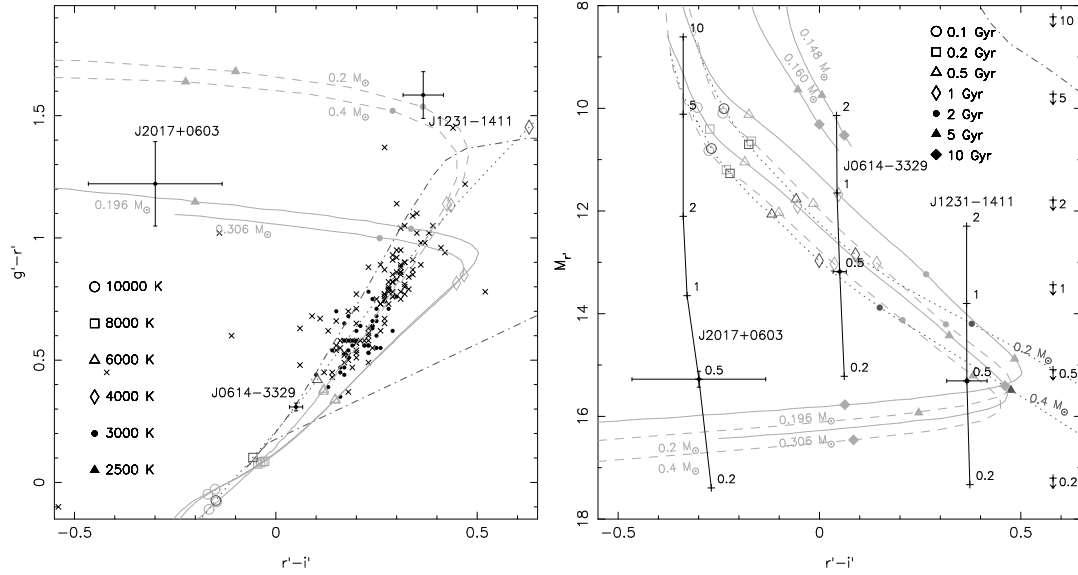


Figure 4. Color-color (*left*) and color-magnitude (*right*) diagrams showing various Helium-core white dwarf cooling tracks. The Rohrmann et al. (2002) models for specific white dwarf masses are plotted as solid lines, while the Bergeron models as described in Holberg & Bergeron (2006); Kowalski & Saumon (2006); Tremblay et al. (2011) and Bergeron et al. (2011) are dashed for white dwarfs with a Hydrogen atmosphere (DA white dwarfs), and dotted for those with Helium atmospheres (DB white dwarfs). The Johnson-Cousins *BVRI* magnitudes from the Rohrmann et al. (2002) model were converted to SDSS *g'r'i'* using the transformations of Smith et al. (2002). The mass of each model is indicated. Models with masses below about $0.2 M_{\odot}$ have thick Hydrogen envelopes and cool slower than models with higher masses. Effective temperatures or cooling ages are indicated along the tracks. The dash-dotted line is a 1 Gyr, solar metallicity isochrone from Girardi et al. (2004) depicting the location of non-degenerate main-sequence stars. In the color-color diagram the colors of ultra-cool white dwarfs from the SDSS (Kilic et al. 2010) are plotted. White dwarfs with spectroscopically determined Hydrogen atmospheres (DA) are plotted with dots; those with non-Hydrogen atmospheres are plotted with crosses (mostly DC type showing no spectral features). The observed $g' - r'$ and $r' - i'$ colors for PSRs J0614–3329, J1231–1411 and J2017+0603 are plotted in the color-color diagram, while $r' - i'$ colors and absolute r' magnitudes ($M_{r'}$) are shown in the color-magnitude diagram. These absolute magnitudes are plotted for various distances indicated by the numbers along the track (distance in kiloparsecs) and corrected for absorption and reddening using the predictions from the Drimmel et al. (2003) model, using extinction coefficients from Schlegel et al. (1998). Finally, limits on the absolute r' magnitude of PSR J0613–0200 are indicated by arrows on the right-hand side of the color-magnitude diagram. Here various distances (in kiloparsecs) are again indicated.

M_c relation between orbital period and companion mass, as predicted by binary evolution, predicts $M_{c,\text{pred}} = 0.299 M_{\odot}$ (Lin et al. 2011). As the inferred mass is lower than that, this may indicate that we observe the system edge on or that the pulsar may be less massive than the assumed $1.4 M_{\odot}$. However, we consider it more likely that the low signal-to-noise of the observed spectrum and degeneracies between the shape of the Balmer lines and the broadening by the slit and seeing leads to unmodelled systematic errors underestimating the surface gravity.

In Fig. 4 we compare the broadband magnitudes of the millisecond pulsar companions against predictions from white dwarf cooling models by Rohrmann et al. (2002) and those by Bergeron et al.² as described in Holberg & Bergeron (2006); Kowalski & Saumon (2006); Tremblay et al. (2011) and Bergeron et al. (2011). Here we used the model for Galactic absorption by Drimmel et al. (2003), which predicts A_V as a function of distance for specific lines of sight. The extinction coefficients by Schlegel et al. (1998) were used to transform A_V into $A_{g'}$, $A_{r'}$ and $A_{i'}$. Because of the high Galactic latitude of the pulsars, the absorption is small; PSR J0613–0200 has the largest maximum absorption of $A_{V,\text{max}} = 0.7$ mag, while PSRs J0614–3329,

J1231–1411 and J2017+0603 have 0.15, 0.13 and 0.46 mag, respectively.

We find that for PSR J0614–3329 the comparison of the broadband colors with cooling models yields a temperature that is consistent with the spectroscopic determination. At these temperatures, the Bergeron and Rohrmann et al. (2002) white dwarf cooling models yield distances in the range of $d = 540$ to 630 pc and white dwarf cooling ages between 1 and 1.5 Gyr.

In the case of PSR J1231–1411 and PSR J2017+0603, the observed colors and magnitudes of the companions are consistent with those expected for cool white dwarfs. Main-sequence companions such as those observed in the “redback” systems can be ruled out; the colors deviate significantly from those of main-sequence stars. For comparison, a $0.2 M_{\odot}$ main-sequence star has $M_{r'} = 11.49$, $g' - i' = 1.42$ and $r' - i' = 0.99$ (Girardi et al. 2004). Furthermore, “redback” systems have severely bloated companions, and the companion to the “redback” PSR J1023+0038 has $r' = 17.43$, which, at a distance of $d = 1.37$ kpc (Deller et al. 2012), would translate to $M_{r'} = 6.75$. If the companions to PSRs J1231–1411 and J2017+0603 had that intrinsic brightness they would be at distances of $d = 28$ kpc, easily ruled out by the dispersion measure distance estimates.

² <http://www.astro.umontreal.ca/~bergeron/CoolingModels/>

Instead, we find that for PSR J1231–1411 and PSR J2017+0603, the $g' - r'$ and $r' - i'$ colors of the companions are located in the part of the color-color diagram where the dominant source of opacity changes from bound-free absorption of H^- at high temperatures to collision-induced absorption of H_2 at lower temperatures (Lenzuni et al. 1991; Saumon et al. 1994; Hansen 1998). The Bergeron and Rohrmann et al. (2002) models diverge here as the latter do not take into account the effect of Ly α absorption on the opacity at blue wavelengths (Kowalski & Saumon 2006). Furthermore, depending on the atmospheric composition of the white dwarf (the He/H abundance ratio) the cooling tracks can level out at $g' - r'$ values ranging from 0.7 to 1.6 (Giammichele et al. 2012, see also Fig. 7 of Parsons et al. 2012). The updated models by Rohrmann et al. (2011) do take into account the absorption by Ly α , but unfortunately only cover white dwarf masses between 0.5 and 0.9 M_\odot , which is above the mass range we expect for the systems studied in this paper.

Despite the uncertainty in the Helium abundance and the predicted $g' - r'$ color, the Bergeron and Rohrmann et al. (2002) cooling models predict comparable temperatures and absolute magnitudes for a given $r' - i'$ color. Taking the predictions at face value, we find that the companions to PSR J1231–1411 and PSR J2017+0603 must be cool ($T_{\text{eff}} \lesssim 3000$ K), old ($\tau_{\text{WD}} \gtrsim 7$ Gyr) and nearby ($d \lesssim 0.5$ kpc).

For PSR J0613–0200, (Desvignes et al. 2015) and Arzoumanian et al. (2015) report a parallax of $\pi = 1.25 \pm 0.13$ mas and $\pi = 0.91 \pm 0.15$ mas, respectively. These translate to Lutz-Kelker bias (Lutz & Kelker 1973; Verbiest et al. 2010) corrected distance estimates of $d = 0.78 \pm 0.08$ kpc and $d = 0.98 \pm 0.16$ kpc. At these distances the non-detection of the white dwarf companion to PSR J0613–0200 sets a lower limit on the absolute r' magnitude of $M_{r'} > 13.9$. This limit excludes the thick Hydrogen atmosphere models by Rohrmann et al. (2002) (those with masses of 0.148, 0.160 and 0.169 M_\odot), which still have $M_V \sim M_{r'} \lesssim 11$ at ages of 15 Gyr. As such, the observations suggest that the companion must have a thin Hydrogen atmosphere and is expected to have temperatures below 5000 K and have cooling ages in excess of 4 Gyr.

4 DISCUSSION AND CONCLUSIONS

We have discovered the binary companions to radio millisecond pulsars J0614–3329, J1231–1411 and J2017+0603, and set limits on the brightness of the companion to PSR J0613–0200.

The spectroscopic observations of the companion to PSR J0614–3329 confirm that the companion is a DA type white dwarf and constrain the temperature to $T_{\text{eff}} = 6460 \pm 80$ K. The surface gravity of $\log g = 7.0 \pm 0.2$ cgs and hence white dwarf mass of $M_{\text{WD}} = 0.24 \pm 0.04 M_\odot$ are low but consistent with expectations based on the orbital parameters of the binary. Comparing the broadband photometry against white dwarf cooling models yields a distance which is a factor 3 to 4 closer than the $d_{\text{DM}} = 1.9$ kpc predicted by the NE2001 model (Cordes & Lazio 2002) based on the observed dispersion measure. Ransom et al. (2011) already noted that the NE2001 model was over estimating the distance to PSR J0614–3329 due to its location at the edge

of the Gum nebula. This reduction in the pulsar distance equally reduces the very high implied γ -ray efficiency of $\eta = 215\%$ (Ransom et al. 2011; Johnson et al. 2014) to more appropriate values of order 17 to 24%.

The distance of the white dwarf companion to PSR J1231–1411 is consistent with the distance estimated from the dispersion measure of the pulsar. In the case of PSR J2017+0603 the white dwarf cooling models place the system at a distance of less than 0.5 kpc. This is considerably closer than the dispersion measure distance of $d_{\text{DM}} = 1.56$ kpc, and consistent with the Lutz & Kelker (1973) bias correct parallax distance of 0.6 ± 0.2 kpc measured from pulsar timing (Guillemot et al. 2015). The distance determined from the white dwarf photometry would reduce the γ -ray efficiency of PSR J2017+0603 to values below 8%.

We find that the companions to PSRs J0613–0200, J1231–1411 and J2017+0603 are old and cool. They are similar in temperature or cooler than the best studied low-mass pulsar companion, that of PSR J0437–4715, for which Durant et al. (2012) derive a temperature of $T_{\text{eff}} = 3950 \pm 150$ K. To cool to these low temperatures the white dwarfs must have thin Hydrogen envelopes to prevent residual Hydrogen burning keeping the white dwarf hot (e.g. Hansen & Phinney 1998). The thickness of the Hydrogen envelope can be reduced by Hydrogen shell flashes. Evolutionary models indicate that Hydrogen shell flashes only occur for white dwarfs with masses above about 0.2 M_\odot , though it is not clear if this is a sharp threshold, leading to a dichotomy in white dwarf cooling properties (Alberts et al. 1996; Driebe et al. 1998; Althaus et al. 2001, 2013), or a smooth transition with white dwarf mass (Istrate et al. 2014).

Besides Hydrogen flashes, irradiation by the pulsar may result in the removal of the Hydrogen envelope when the companion detaches from the Roche lobe. This scenario has been proposed for PSR J0751+1807 by Ergma et al. (2001) to explain the low temperature of its white dwarf companion. For this pulsar, Shapiro delay measurements yield a white dwarf mass of 0.16 M_\odot (Nice et al. 2008; Desvignes et al. 2015), below the mass threshold where no Hydrogen flashes are expected to occur, yet observations of the companion by Bassa et al. (2006a) show that it is cool ($T_{\text{eff}} \approx 4000$ K) and faint, ruling out the presence of a thick Hydrogen envelope.

For the companion to PSR J0613–0200, and perhaps the companions to PSRs J1231–1411 and J2017+0603 irradiation by the pulsar wind may be, or may have been, important. In Figure 5 we compare the companion flux ($f_c = \sigma T_{\text{eff}}^4$) to the flux of the pulsar wind irradiating the companion surface for all known optical companions ($f_{\text{irr}} = L_{\text{SD}}/4\pi a^2$, where $L_{\text{SD}} \propto \dot{P}/P^3$ is the pulsar spin-down luminosity and a is orbital separation). We find that these three systems, as well as PSR J0751+1807, and possibly J0034–0534, are located in the region where $f_c \approx f_{\text{irr}}$. Systems which are clearly irradiated, like the ‘black widow’ and ‘redback’ pulsars, fall in the region where $f_c < f_{\text{irr}}$, while systems with spectroscopically constrained white dwarf temperatures have $f_c > f_{\text{irr}}$.

Theoretical modelling of the binary evolution of short orbital period neutron stars has revealed that irradiation plays a major role in the formation of the ‘black widow’ and ‘redback’ systems (Pfahl et al. 2003; Chen et al. 2013; Benvenuto et al. 2014, 2015a,b). After the companion decou-

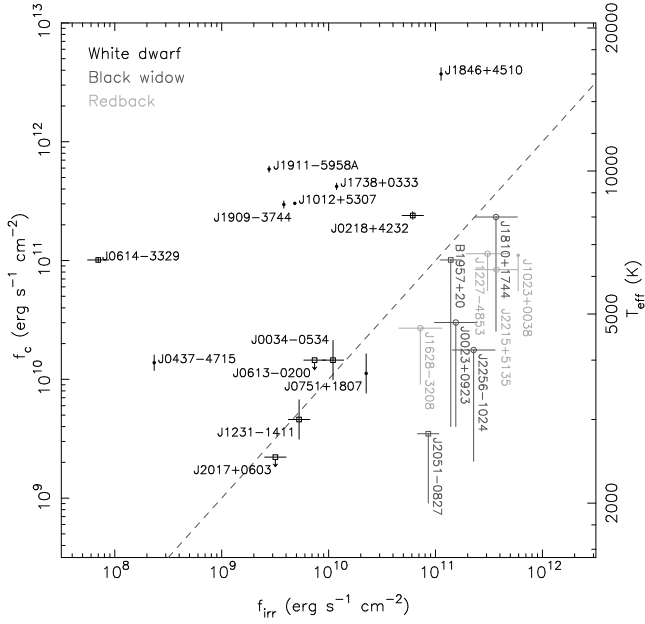


Figure 5. A comparison between the flux of the companion f_c and the flux of the pulsar wind irradiating the companion f_{irr} for pulsar binaries where accurate companion temperatures are available. The spindown luminosity has used spin period derivatives corrected for the apparent acceleration due to proper motion (the Shklovskii 1970 effect) where available. The binary separation a is taken for the median companion mass (inclination $i = 60^\circ$) if no mass measurements are available. In the case of known proper motions and binary masses, the points are indicated with black dots. If only proper motions are known, open circles are used and a 10% uncertainty on the spindown luminosity is assumed. If neither proper motion nor binary masses are known, a 20% uncertainty is assumed. The companion types are as indicated, while the dashed diagonal line depicts $f_c = f_{irr}$. Companion temperatures and pulsar parameters are from van Kerkwijk et al. (1996); Lundgren et al. (1996); Callanan et al. (1998); Bassa et al. (2003, 2006a,b); Durant et al. (2012); Jacoby et al. (2003); Antoniadis et al. (2012); Kaplan et al. (2013); Breton et al. (2013); Thorstensen & Armstrong (2005); Stappers et al. (1999); Li et al. (2014); de Martino et al. (2014) and the ATNF pulsar catalogue (Manchester et al. 2005).

ples from the Roche lobe, the pulsar mechanism switches on and starts irradiating the companion, leading to mass loss through evaporation. The efficiency of the irradiation and evaporation determines the mass loss. These models allow for the possibility suggested by Ergma et al. (2001); that (part of) the Hydrogen envelope is lost due to irradiation after the companion detaches from the Roche lobe.

Though the white dwarf companions to PSRs J0613–0200, J1231–1411 and J2017+0603 may have had their Hydrogen envelopes reduced through Hydrogen flashes, we can not rule out the possibility of mass loss due to irradiation. A search for photometric variability for PSRs J1231–1411 and J2017+0603 may constrain the effects of irradiation in these objects.

ACKNOWLEDGMENTS

We thank the anonymous referee for useful suggestions, and thank Marten van Kerkwijk, Thomas Tauris and Alina Istrate for helpful discussions. CGB acknowledges the hospitality of the International Space Science Institute (ISSI) in Bern, Switzerland. Based on observations made with ESO Telescopes at the La Silla Paranal Observatory under programme ID 088.D-0138 and on observations obtained at the Gemini Observatory (Program ID GS-2010B-Q-56), which is operated by the Association of Universities for Research in Astronomy, Inc., under a cooperative agreement with the NSF on behalf of the Gemini partnership: the National Science Foundation (United States), the National Research Council (Canada), CONICYT (Chile), the Australian Research Council (Australia), Ministério da Ciência, Tecnologia e Inovação (Brazil) and Ministerio de Ciencia, Tecnología e Innovación Productiva (Argentina). CGB acknowledges support from the European Research Council under the European Union’s Seventh Framework Programme (FP/2007-2013) / ERC Grant Agreement nr. 337062 (DRAGNET; PI Jason Hessels).

REFERENCES

- Alberts F., Savonije G. J., van den Heuvel E. P. J., Pols O. R., 1996, *Nature*, **380**, 676
- Althaus L. G., Serenelli A. M., Benvenuto O. G., 2001, *MNRAS*, **324**, 617
- Althaus L. G., Miller Bertolami M. M., Córscico A. H., 2013, *A&A*, **557**, A19
- Antoniadis J., van Kerkwijk M. H., Koester D., Freire P. C. C., Wex N., Tauris T. M., Kramer M., Bassa C. G., 2012, *MNRAS*, **423**, 3316
- Archibald A. M., et al., 2009, *Science*, **324**, 1411
- Arzoumanian Z., et al., 2015, preprint, ([arXiv:1505.07540](https://arxiv.org/abs/1505.07540))
- Barr E. D., et al., 2013, *MNRAS*, **435**, 2234
- Bassa C. G., van Kerkwijk M. H., Kulkarni S. R., 2003, *A&A*, **403**, 1067
- Bassa C. G., van Kerkwijk M. H., Kulkarni S. R., 2006a, *A&A*, **450**, 295
- Bassa C. G., van Kerkwijk M. H., Koester D., Verbunt F., 2006b, *A&A*, **456**, 295
- Bassa C. G., et al., 2014, *MNRAS*, **441**, 1825
- Benvenuto O. G., De Vito M. A., Horvath J. E., 2014, *ApJ*, **786**, L7
- Benvenuto O. G., De Vito M. A., Horvath J. E., 2015a, *MNRAS*, **449**, 4184
- Benvenuto O. G., De Vito M. A., Horvath J. E., 2015b, *ApJ*, **798**, 44
- Bergeron P., et al., 2011, *ApJ*, **737**, 28
- Boyles J., et al., 2013, *ApJ*, **763**, 80
- Breton R. P., et al., 2013, *ApJ*, **769**, 108
- Callanan P. J., Garnavich P. M., Koester D., 1998, *MNRAS*, **298**, 207
- Chen H.-L., Chen X., Tauris T. M., Han Z., 2013, *ApJ*, **775**, 27
- Cognard I., et al., 2011, *ApJ*, **732**, 47
- Cordes J. M., Lazio T. J. W., 2002, preprint, ([arXiv:0207156](https://arxiv.org/abs/0207156))
- Cordes J. M., et al., 2006, *ApJ*, **637**, 446
- Deller A. T., et al., 2012, *ApJ*, **756**, L25
- Desvignes G., Caballero R. N., Lentati L., Verbiest J. P. W., Janssen G. H., Desvignes G., 2015, in prep.
- Driebe T., Schönberner D., Blöcker T., Herwig F., 1998, *A&A*, **339**, 123

- Drimmel R., Cabrera-Lavers A., López-Corredoira M., 2003, *A&A*, **409**, 205
- Durant M., Kargaltsev O., Pavlov G. G., Kowalski P. M., Posselt B., van Kerkwijk M. H., Kaplan D. L., 2012, *ApJ*, **746**, 6
- Ergma E., Sarna M. J., Gerškevičs-Antipova J., 2001, *MNRAS*, **321**, 71
- Fukugita M., Ichikawa T., Gunn J. E., Doi M., Shimasaku K., Schneider D. P., 1996, *AJ*, **111**, 1748
- Giammichele N., Bergeron P., Dufour P., 2012, *ApJS*, **199**, 29
- Girardi L., Grebel E. K., Odenkirchen M., Chiosi C., 2004, *A&A*, **422**, 205
- Guillemot L., Smith D. A., Laffon H., Cognard I., Janssen G. H., Desvignes G., 2015, in prep.
- Hansen B. M. S., 1998, *Nature*, **394**, 860
- Hansen B. M. S., Phinney E. S., 1998, *MNRAS*, **294**, 557
- Hessels J. W. T., Ransom S. M., Kaspi V. M., Roberts M. S. E., Champion D. J., Stappers B. W., 2008, in Bassa C., Wang Z., Cumming A., Kaspi V. M., eds, *American Institute of Physics Conference Series Vol. 983, 40 Years of Pulsars: Millisecond Pulsars, Magnetars and More*. pp 613–615 ([arXiv:0710.1745](https://arxiv.org/abs/0710.1745)), doi:10.1063/1.2900310
- Holberg J. B., Bergeron P., 2006, *AJ*, **132**, 1221
- Horne K., 1986, *PASP*, **98**, 609
- Hynes R. I., 2002, *A&A*, **382**, 752
- Istrate A. G., Tauris T. M., Langer N., Antoniadis J., 2014, *A&A*, **571**, L3
- Jacoby B. A., Bailes M., van Kerkwijk M. H., Ord S., Hotan A., Kulkarni S. R., Anderson S. B., 2003, *ApJ*, **599**, L99
- Johnson T. J., et al., 2014, *ApJS*, **213**, 6
- Kaplan D. L., Bhalariao V. B., van Kerkwijk M. H., Koester D., Kulkarni S. R., Stovall K., 2013, *ApJ*, **765**, 158
- Keith M. J., et al., 2010, *MNRAS*, **409**, 619
- Kilic M., et al., 2010, *ApJS*, **190**, 77
- Koester D., 2010, *Mem. Soc. Astron. Italiana*, **81**, 921
- Kowalski P. M., Saumon D., 2006, *ApJ*, **651**, L137
- Lenzuni P., Chernoff D. F., Salpeter E. E., 1991, *ApJS*, **76**, 759
- Li M., Halpern J. P., Thorstensen J. R., 2014, *ApJ*, **795**, 115
- Lin J., Rappaport S., Podsiadlowski P., Nelson L., Paxton B., Todorov P., 2011, *ApJ*, **732**, 70
- Lorimer D. R., et al., 1995, *ApJ*, **439**, 933
- Lundgren S. C., Foster R. S., Camilo F., 1996, in *ASP Conf. Ser. 105: IAU Colloq. 160: Pulsars: Problems and Progress*. p. 497
- Lutz T. E., Kelker D. H., 1973, *PASP*, **85**, 573
- Manchester R. N., Hobbs G. B., Teoh A., Hobbs M., 2005, *AJ*, **129**, 1993
- Monet D. G., et al., 2003, *AJ*, **125**, 984
- Nice D. J., Stairs I. H., Kasian L. E., 2008, in Bassa C., Wang Z., Cumming A., Kaspi V. M., eds, *American Institute of Physics Conference Series Vol. 983, 40 Years of Pulsars: Millisecond Pulsars, Magnetars and More*. pp 453–458, doi:10.1063/1.2900273
- Panei J. A., Althaus L. G., Chen X., Han Z., 2007, *MNRAS*, **382**, 779
- Papitto A., et al., 2013, *Nature*, **501**, 517
- Parsons S. G., et al., 2012, *MNRAS*, **426**, 1950
- Pfahl E., Rappaport S., Podsiadlowski P., 2003, *ApJ*, **597**, 1036
- Ransom S. M., 2013, in *IAU Symposium*. pp 3–10 ([arXiv:1211.3138](https://arxiv.org/abs/1211.3138)), doi:10.1017/S1743921312023046
- Ransom S. M., et al., 2011, *ApJ*, **727**, L16+
- Ray P. S., et al., 2012, preprint, ([arXiv:1205.3089](https://arxiv.org/abs/1205.3089))
- Roberts M. S. E., 2013, in *IAU Symposium*. pp 127–132 ([arXiv:1210.6903](https://arxiv.org/abs/1210.6903)), doi:10.1017/S174392131202337X
- Rohrman R. D., Serenelli A. M., Althaus L. G., Benvenuto O. G., 2002, *MNRAS*, **335**, 499
- Rohrman R. D., Althaus L. G., Kepler S. O., 2011, *MNRAS*, **411**, 781
- Saumon D., Bergeron P., Lunine J. I., Hubbard W. B., Burrows A., 1994, *ApJ*, **424**, 333
- Schlegel D. J., Finkbeiner D. P., Davis M., 1998, *ApJ*, **500**, 525
- Shklovskii I. S., 1970, *Soviet Astronomy*, **13**, 562
- Skrutskie M. F., et al., 2006, *AJ*, **131**, 1163
- Smith J. A., et al., 2002, *AJ*, **123**, 2121
- Stappers B. W., van Kerkwijk M. H., Lane B., Kulkarni S. R., 1999, *ApJ*, **510**, L45
- Stetson P. B., 1987, *PASP*, **99**, 191
- Tauris T. M., Savonije G. J., 1999, *A&A*, **350**, 928
- Thorstensen J. R., Armstrong E., 2005, *AJ*, **130**, 759
- Tremblay P.-E., Bergeron P., Gianninas A., 2011, *ApJ*, **730**, 128
- Verbiest J. P. W., Lorimer D. R., McLaughlin M. A., 2010, *MNRAS*, **405**, 564
- de Martino D., et al., 2014, *MNRAS*, **444**, 3004
- van Kerkwijk M. H., Bergeron P., Kulkarni S. R., 1996, *ApJ*, **467**, L89
- van Kerkwijk M. H., Bassa C. G., Jacoby B. A., Jonker P. G., 2005, in Rasio F. A., Stairs I. H., eds, *ASP Conference Series Vol. 328, Binary Radio Pulsars*. ASP, p. 357

This paper has been typeset from a \LaTeX file prepared by the author.